


 Cite this: *Chem. Commun.*, 2021, 57, 5678

 Received 16th December 2020,
 Accepted 4th May 2021

DOI: 10.1039/d0cc08156f

rsc.li/chemcomm

In vitro studies of deferasirox derivatives as potential organelle-targeting traceable anti-cancer therapeutics†

 Axel Steinbrueck,^a Adam C. Sedgwick,^a Hai-Hao Han,^b Michael Y. Zhao,^a Sajal Sen,^a Dan-Ying Huang,^a Yi Zang,^c Jia Li,^{*c} Xiao-Peng He^{*b} and Jonathan L. Sessler^{ib,*a}

We report here strategic functionalization of the FDA approved chelator deferasirox (**1**) in an effort to produce organelle-targeting iron chelators with enhanced activity against A549 lung cancer cells. Derivative **8** was found to have improved antiproliferative activity relative to **1**. Fluorescent cell imaging revealed that compound **8** preferentially localises within the lysosome.

Over the past decades, iron chelators have gained increasing attention as potential primary or adjuvant cancer therapies.^{1–4} The depletion of iron from rapidly proliferating cancer cells has been shown to result in effective growth inhibition and to ultimately induce apoptotic cell death.^{5–7} Within this arena, the clinical iron sequestration agent deferasirox (**1**, Scheme 1) has shown encouraging initial anticancer activity *in vitro* and *in vivo* for example against *inter alia* AML,⁸ triply negative breast cancer,⁹ and lung cancer.^{10,11} Despite this promise, the treatment of solid tumours with **1** remains challenging and new chelators are required that are taken up into cancerous cells efficiently and which display enhanced cytotoxicity.^{12,13} Only a few reports are currently available in the literature that discuss the derivatization of **1** to produce anticancer agents, and the majority of derivatives synthesized in such a context show only moderate cytotoxicity *in vitro* with concentrations >100 μM required to achieve baseline eradication of cancer cells.^{14–16}

To address these challenges, our efforts have focused on the development of chelators that show enhanced cytotoxicity and produce a steep, non-plateauing dose–response curve, a property that is considered favourable for chemotherapeutics. This is because small, clinically achievable increases in the concentration of a drug above its IC₅₀ value can translate into a disproportionately larger fractional killing of cancer cells.^{17,18}

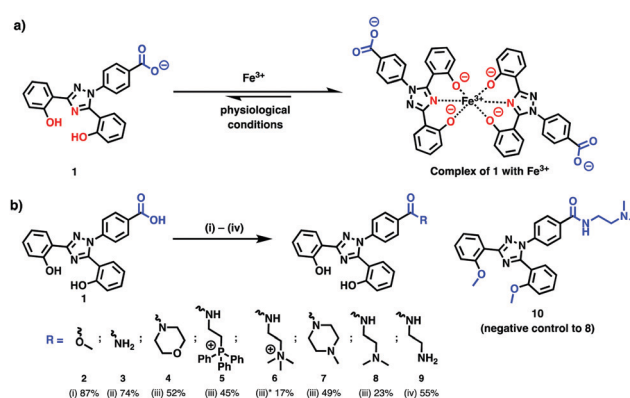
A design feature of **1** that limits its efficacy as an anticancer agent is the terminal carboxylic acid (highlighted in blue in Scheme 1), which imparts an overall negative charge on this ligand at physiological pH, thereby disfavoring the effective passage of **1** through lipid cell membranes.¹⁹ To ameliorate the above-mentioned drawback of **1** we have investigated the strategic derivatization of the carboxylic acid *via* introduction of organelle targeting groups designed to improve cellular uptake while guiding preferential localization within the lysosome or mitochondria.^{20,21} These latter organelles constitute

^a Department of Chemistry, University of Texas at Austin, 105 E 24th street A5300, Austin, TX 78712-1224, USA. E-mail: sessler@cm.utexas.edu

^b Key Laboratory for Advanced Materials and Joint International Research Laboratory of Precision Chemistry and Molecular Engineering, Feringa Nobel Prize Scientist Joint Research Center, Frontiers Center for Materiobiology and Dynamic Chemistry, School of Chemistry and Molecular Engineering, East China University of Science and Technology, 130 Meilong Rd., Shanghai 200237, China. E-mail: xphe@ecust.edu.cn

^c National Center for Drug Screening, State Key Laboratory of Drug Research, Shanghai Institute of Materia Medica, Chinese Academy of Sciences, Shanghai 201203, P. R. China. E-mail: jli@simm.ac.cn

† Electronic supplementary information (ESI) available. See DOI: 10.1039/d0cc08156f



Scheme 1 (a) Structures of **1** and its complex with Fe³⁺. The donor set is highlighted in red and the carboxylate moiety is highlighted in blue. (b) Conditions: (i) Methanol, reflux, 48 h. (ii) Urea (4 equiv.), imidazole (2 equiv.), microwave 150 W, 170 °C, 20 min. (iii) EDC (2 equiv.), TEA (2 equiv.), NHS (cat.), amine (3 equiv.), CH₂Cl₂, r.t., 16 h. (iv) Same as (iii) with N-BOC ethylenediamine, then TFA, r.t., 16 h.

appealing targets due to their key role in mediating intracellular iron metabolism and their reported sensitivity to iron chelation therapy, which is thought to be mediated *via* the induction of oxidative stress caused by ROS generation in these organelles, for example, in the cases of the potent iron chelators salinomycin and Dp44mT, respectively.^{6,20–23}

We have now examined the antiproliferative activity of several new derivatives of **1** using the A549 human lung cancer cell line and as detailed below identified derivative **8** as having an enhanced therapeutic activity compared to **1**. In contrast to deferasirox, **8** proved fluorescent in aqueous environments, which allowed its subcellular localisation in the lysosome to be followed by fluorescent microscopy.

First, guided by the premise that they would benefit from improved passive diffusion through lipid membranes and thus faster internalization with respect to **1**, derivatives with neutral sidechains were prepared (compounds **2–4**, Scheme 1b). Next, we synthesized derivatives containing hydrophilic amine and ammonium side chains (**6–9**, Scheme 1b) as these functionalities have been reported to promote preferential localisation in the lysosome.²⁴ Finally, we prepared one derivative (**5**, Scheme 1b) with a cationic triphenylphosphonium moiety, a hydrophobic subunit reported to drive localisation toward the mitochondria.^{20,25} Detailed synthetic procedures for all compounds prepared in this study, as well as their respective characterization by ¹H- and ¹³C-NMR spectroscopy and high resolution mass spectrometry, are available in the ESI†. All new derivatives were found to be stable under physiological conditions at 37 °C over the course of several days (*cf.* ESI†). The lipophilicity of **1–9** was quantified by determining their distribution coefficients (log D) at pH 7.2 and at pH 4.5 (to mimic lysosomal pH) (*cf.* Table S1 in the ESI†). In accord with the design expectations, the lipophilicity of the carboxylic acid **1** increased at lower pH while the amine derivatives became more hydrophilic in more acidic environments.

The antiproliferative activity of compounds **1–9** and control **10** was evaluated in A549 lung cancer cells, a cell line with a well-established sensitivity to iron imbalance.^{11,26} The clinical chemotherapeutic oxaliplatin (Ox-Pt) with a known activity profile in A549 cells was included as a positive control.^{27,28} For each compound, cellular proliferation profiles were produced *via* a standard MTT assay for exposure times of 72 h and 24 h, respectively (*cf.* Fig. S1 and S2 in the ESI†). From these proliferation profiles, averaged IC₅₀ values and Hill slope (HS) parameters were determined *via* nonlinear regression analysis. The results are summarised in Table 1. IC₅₀ values represent a commonly reported metric of toxicity, while HS parameters provide insight into the shape of the proliferation profile, wherein higher HS values are desirable as they correspond to a steeper dose–response curve. HS values have attracted interest in recent years as this parameter was found to exhibit greater consistency when compared across different cell lines than the IC₅₀ value.¹⁷

The determined IC₅₀ values of **1** and Ox-Pt are in good agreement with previous literature reports for an exposure time of 72 h.^{11,27} At 72 h incubation time, the new derivatives of this

Table 1 IC₅₀ and Hill slope (HS) values for **1–10** against the A549 human lung cancer cell line after 72 h and 24 h incubation. Experiments were performed in triplicate

Compound	IC ₅₀ (72 h)	HS (72 h)	IC ₅₀ (24 h)	HS (24 h)
Ox-Pt	0.5 ± 0.1 μM	1.2 ± 0.2	> 50 μM	N/A
1	8.5 ± 2.0 μM	1.0 ± 0.2	> 50 μM	N/A
2	2.5 ± 0.7 μM	0.9 ± 0.2	21.0 ± 3.0 μM	1.3 ± 0.2
3	8.3 ± 2.2 μM	0.8 ± 0.2	> 50 μM	N/A
4	3.6 ± 1.6 μM	0.6 ± 0.2	> 50 μM	N/A
5	6.0 ± 0.6 μM	1.9 ± 0.3	29.0 ± 1.4 μM	2.9 ± 0.6
6	> 50 μM	N/A	> 50 μM	N/A
7	3.8 ± 0.5 μM	1.0 ± 0.1	23.3 ± 1.5 μM	1.8 ± 0.2
8	3.7 ± 0.3 μM	2.7 ± 0.6	12.3 ± 1.3 μM	3.5 ± 1.0
9	7.7 ± 0.8 μM	1.7 ± 0.3	12.6 ± 0.8 μM	2.7 ± 0.4
10	> 50 μM	N/A	> 50 μM	N/A

study showed activities that were either improved relative to **1** or similar. The exception was **6**, which proved inactive. Reducing the exposure time to 24 h decreased the apparent activity of the charge neutral derivatives **2–4**, as well as Ox-Pt by over an order of magnitude. This finding leads us to suggest that several cell cycles are required for these compounds to exert a cytotoxic effect. Interestingly, the activity of the derivatives with lysosomal targeting amine groups **7**, **8** and **9**, were less impacted by shorter exposure times with **8** (IC₅₀ = 12.3 μM) and **9** (IC₅₀ = 12.6 μM) exhibiting the highest activity under these conditions. Compounds **8** and **9** furthermore produced the highest HS parameters after both 72 h and 24 h exposures, while **1**, Ox-Pt, and the derivatives with neutral side chains (*i.e.*, **2–4**) produced rather shallow dose–response curves (Table 1) and required concentrations ≥ 100 μM to achieve baseline eradication of A549 cancer cells. The determined IC₅₀ values of the potent derivatives **2** and **8**, as well as **5** bearing a mitochondria directing group, were verified *via* crystal violet staining as a secondary measure of activity. In all cases, IC₅₀ values close to those determined *via* MTT assay were obtained (*cf.* Fig. S6 in the ESI†).²⁹

Comparison studies for derivatives **2** and **8**, as well as the parent chelator **1**, in HCT116 colon cancer cells and L929 non-cancerous mouse fibroblast cells showed consistent activity for each chelator, respectively, across all three cell lines (*cf.* Fig. S5 in the ESI† for proliferation profiles and Table S2 for IC₅₀ values). These results were taken as evidence that the cell type did not significantly affect the activity of the present iron chelators. The combination of favourable cytotoxicity and HS seen at 72 h in the case of **8** led us to prepare its diether analogue **10** *via* methylation of the phenol moieties (*cf.* ESI† Scheme S1). This derivative was expected to display a reduced metal binding affinity thus serving as a negative control for **8**. In fact, derivative **10** exerted no appreciable antiproliferative activity against A549 cells under conditions identical to those used to test compounds **1–9** as shown in Fig. 1. Additionally, when cells were supplemented with 50 μM FeCl₃, both **1** and **8** no longer produced any observable cytotoxicity after 72 h of exposure (*cf.* Fig. S3 in the ESI†). This finding is taken as evidence that intracellular iron chelation plays a key role in mediating their *in vitro* antiproliferative activity.

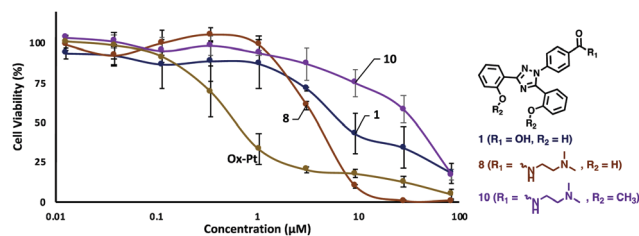


Fig. 1 Selected proliferation profiles of **1**, **8**, **10** and oxaliplatin (Ox-Pt) in A549 cells. The high HS parameter of **8** translates to sharp decline in cell viability with increasing drug concentration. Derivative **8** also achieves baseline eradication of cancer cells at the lowest concentration of all evaluated drugs. See text for discussion.

In contrast to deferasirox **1**, derivatives **2** and **8** at concentrations of 50 μM give rise to distinct fluorescence emission bands centred 510 nm and 480 nm, respectively, in PBS (*cf.* Fig. S9–S11, ESI[†]). This allowed their subcellular location to be explored with the results shown in Fig. 2. As confirmed by comparisons with LysoTracker[®] red, derivative **8** was found to localise in the lysosome as determined by fluorescent cell microscopy using A549 cells. In contrast, no discernible organelle targeting was seen in the case of **2**, a chelator that lacks a recognized organelle targeting unit. The enhanced cytotoxicity and localization in the lysosome seen for **8** proved reproducible in HeLa cells (*cf.* Fig. S12 in the ESI[†]).

No detectable increase in ROS production was seen in A549 cells after incubation with the potent derivative **8** as evidenced by confocal microscopy (*cf.* Fig. S13 in the ESI[†]). These results lead us to suggest that the enhanced therapeutic efficacy seen in the case of **8** is due, at least in part, to its intracellular localization and that the cytotoxicity of this derivative is exerted *via* an ROS-independent mechanism. This sets **8** apart from other lysosome directed iron chelators, such as salinomycin.²¹

We further utilized the fluorescent properties of the triphenylphosphonium-bearing derivative **5** to trace successfully this chelator inside A549 cells (*cf.* ESI[†] Fig. S13). However, no colocalization with Mitotracker[®] red was observed for **5**, which may in part explain the low activity of this derivative. Notably, the inherent fluorescent properties of this derivative leads us to conclude that introduction of a well-established mitochondria directing group^{20,25} does not necessarily produce

a mitochondrial localisation effect in the case of simple deferasirox derivatives and that other factors may govern the intracellular distribution of this class of chelator.

Our recent efforts have focused on overcoming the observed unwanted cytotoxicity towards healthy cells. We found, for instance, that deferasirox derivatives can be effectively encapsulating into the ubiquitous blood protein human serum albumin (HSA), an established tumour localizing agent.^{30,31} The parent ligand **1**, as well as the potent derivatives **2** and **8**, were found to bind to HSA as inferred from Stern–Volmer analyses (*cf.* Fig. S6–S8 for the titration data and Table S3 for the Stern–Volmer quenching constants, ESI[†]). The resulting HSA-complexes of **2** and **8**, respectively, showed a 2- and 3-fold increase in cytotoxicity in A549 cells relative to the uncomplexed chelators (*cf.* Fig. S5 for proliferation profiles and Table S2 in the ESI[†] for IC₅₀ values). Encouraged by these results, our future efforts will focus on exploring the tumour targeted delivery of deferasirox derivatives.

In conclusion, we report the synthesis of eight new derivatives of deferasirox including examples with neutral, cationic and amine-containing side chains. These derivatives were evaluated for their antiproliferative activity in A549 cells after incubation times of 24 h and 72 h. The derivatives that contained lysosome targeting moieties, such as **8**, were found to exert notable cytotoxicity after 24 h exposure time and also showed steeper dose–response curves with respect to the parent chelator **1**. Derivative **8**, as well as the majority of the new compounds reported here, proved fluorescent in aqueous media (Fig. S4–S6, ESI[†]), allowing their subcellular localisation to be tracked inside live cells. It was found that the chelator **8**, but not the control system **2** lacking a localising functionality, localised well to the lysosome. The ability to produce an antiproliferative response as well as providing for fluorescence-based tracking, are considered attractive features of the present systems and serve to underscore the versatility of the deferasirox platform in terms of potential iron chelation-based approaches to anticancer drug discovery. More broadly, the present results highlight the benefits that can accrue by optimizing the drug-like properties and targeting features of chelators displaying therapeutic potential.

The initial work in Austin was supported by the National Institutes of Health (grant CA 68682 to J. L. S.). Subsequent studies were supported by the Robert A. Welch Foundation (grant F-0018 to J. L. S.). X.-P. H. thank the NSFC (no. 91853201), the Shanghai Municipal Science and Technology Major Project (2018SHZDZX03), the National Key Sci-Tech Special Projects of Infection Diseases of China (2018ZX10732202) and the International Cooperation Program of Shanghai Science and Technology Committee (17520750100). H.-H. H. would like to thank the China Postdoctoral Science Foundation (No. 2020M681196) for support.

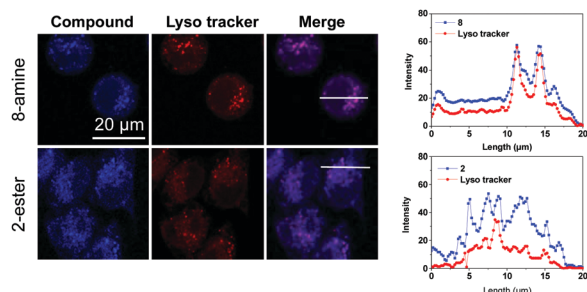


Fig. 2 Confocal microscopy imaging of **2** and **8** (20 μM) in A549 cells. Colocalization was observed between **8** and LysoTracker[®] red. Blue channel: Ex/Em = 405/440–480 nm. Red channel: Ex/Em = 559/580–620 nm.

Conflicts of interest

The authors declare that they have no known competing financial interests or personal relationships that could have appeared to influence the work reported in this paper.

References

- 1 A. Steinbrueck, A. C. Sedgwick, J. T. Brewster, K.-C. Yan, Y. Shang, D. M. Knoll, G. I. Vargas-Zuñiga, X.-P. He, H. Tian and J. L. Sessler, *Chem. Soc. Rev.*, 2020, **49**, 3726–3747.
- 2 J. L. Heath, J. M. Weiss, C. P. Lavau and D. S. Wechsler, *Nutrients*, 2013, **5**, 2836–2859.
- 3 S. V. Torti and F. M. Torti, *Nat. Rev. Cancer*, 2013, **13**, 342–355.
- 4 K. Gaur, A. M. Vázquez-Salgado, G. Duran-Camacho, I. Dominguez-Martinez, J. A. Benjamín-Rivera, L. Fernández-Vega, L. Carmona Sarabia, A. Cruz García, F. Pérez-Deliz, J. A. Méndez Román, M. Vega-Cartagena, S. A. Loza-Rosas, X. Rodriguez Acevedo and A. D. Tinoco, *Inorganics*, 2018, **6**(4), 1–38.
- 5 M. R. Bedford, S. J. Ford, M. Hons, R. D. Horniblow, T. H. Iqbal and C. Tselepis, *J. Clin. Pharmacol.*, 2013, **53**, 885–891.
- 6 M. Fryknäs, X. Zhang, U. Bremberg, W. Senkowski, M. H. Olofsson, P. Brandt, I. Persson, P. D'Arcy, J. Gullbo, P. Nygren, L. K. Schughart, S. Linder and R. Larsson, *Sci. Rep.*, 2016, **6**, 1–11.
- 7 D. Duarte, E. D. Hawkins, O. Akinduro, H. Ang, K. De Filippo, I. Y. Kong, M. Haltali, N. Ruiivo, L. Straszkowski, S. J. Vervoort, C. McLean, T. S. Weber, R. Khorshed, C. Pirillo, A. Wei, S. K. Ramasamy, A. P. Kusumbe, K. Duffy, R. H. Adams, L. E. Purton, L. M. Carlin and C. Lo Celso, *Cell Stem Cell*, 2018, **22**, 64–77.e6.
- 8 C. Callens, S. Coulon, J. Naudin, I. Radford-Weiss, N. Boissel, E. Raffoux, P. H. M. Wang, S. Agarwal, H. Tamouza, E. Paubelle, V. Asnafi, J. A. Ribeil, P. Dessen, D. Canioni, O. Chandesris, M. T. Rubio, C. Beaumont, M. Benhamou, H. Dombret, E. Macintyre, R. C. Monteiro, I. C. Moura and O. Hermine, *J. Exp. Med.*, 2010, **207**, 731–750.
- 9 S. Tury, F. Assayag, F. Bonin, S. Chateau-Joubert, J.-L. Servely, S. Vacher, V. Becette, M. Caly, A. Rapinat, D. Gentien, P. de la Grange, A. Schnitzler, F. Lallemand, E. Marangoni, I. Bièche and C. Callens, *J. Pathol.*, 2018, **246**, 103–114.
- 10 G. Y. L. L. Lui, P. Obeidy, S. J. Ford, C. Tselepis, D. M. Sharp, P. J. Jansson, D. S. Kalinowski, Z. Kovacevic, D. B. Lovejoy and D. R. Richardson, *Mol. Pharmacol.*, 2013, **83**, 179–190.
- 11 S. A. Loza-Rosas, A. M. Vázquez-Salgado, K. I. Rivero, L. J. Negrón, Y. Delgado, J. A. Benjamín-Rivera, A. L. Vázquez-Maldonado, T. B. Parks, C. Munet-Colón and A. D. Tinoco, *Inorg. Chem.*, 2017, **56**, 7788–7802.
- 12 M. Jung, C. Mertens, E. Tomat and B. Brüne, *Int. J. Mol. Sci.*, 2019, **20**, 1–18.
- 13 I. Saeki, N. Yamamoto, T. Yamasaki, T. Takami, M. Maeda, K. Fujisawa, T. Iwamoto, T. Matsumoto, I. Hidaka, T. Ishikawa, K. Uchida, K. Tani and I. Sakaida, *World J. Gastroenterol.*, 2016, **22**, 8967–8977.
- 14 S. Salehi, A. S. Saljooghi and A. Shiri, *Eur. J. Pharmacol.*, 2016, **781**, 209–217.
- 15 P. Rouge, A. Dassonville-Klimpt, C. Cézard, S. Boudesocque, R. Ourouda, C. Amant, F. Gaboriau, I. Forfar, J. Guillon, E. Guillon, E. Vanquelef, P. Cieplak, F. Y. Dupradeau, L. Dupont and P. Sonnet, *ChemPlusChem*, 2012, **77**, 1001–1016.
- 16 M. Theerasilp, P. Chalermpanapun, K. Ponlamuangdee, D. Sukvanitvichai and N. Nasongkla, *RSC Adv.*, 2017, **7**, 11158–11169.
- 17 M. Fallahi-Sichani, S. Honarnejad, L. M. Heiser, J. W. Gray and P. K. Sorger, *Nat. Chem. Biol.*, 2013, **9**, 708–714.
- 18 J. L. Jenkins, *Nat. Chem. Biol.*, 2013, **9**, 669–670.
- 19 X. P. Huang, M. Spino and J. J. Thiessen, *Pharm. Res.*, 2006, **23**, 280–290.
- 20 J. Zielonka, J. Joseph, A. Sikora, M. Hardy, O. Ouari, J. Vasquez-Vivar, G. Cheng, M. Lopez and B. Kalyanaraman, *Chem. Rev.*, 2017, **117**, 10043–10120.
- 21 T. T. Mai, A. Hamaï, A. Hienzsch, T. Cañeque, S. Müller, J. Wicinski, O. Cabaud, C. Leroy, A. David, V. Acevedo, A. Ryo, C. Ginestier, D. Birnbaum, E. Charafe-jauffret, P. Codogno, M. Mehrpour and R. Rodriguez, *Nat. Chem.*, 2017, **9**, 1025–1033.
- 22 A. R. Bogdan, M. Miyazawa, K. Hashimoto and Y. Tsuji, *Trends Biochem. Sci.*, 2016, **41**, 274–286.
- 23 A. M. Merlot, S. Sahni, D. J. R. Lane, A. M. Fordham, N. Pantarat, D. E. Hibbs, V. Richardson, M. R. Doddareddy, J. A. Ong, M. L. H. Huang, D. R. Richardson and D. S. Kalinowski, *Oncotarget*, 2015, **6**, 10374–10398.
- 24 L. Graff, F. Castrop, M. Bauer, H. Höfler and M. Gratzl, *Cancer Res.*, 2001, **61**, 2138–2144.
- 25 R. Y. P. Alta, H. A. Vitorino, D. Goswami, M. Terêsa Machini and B. P. Espósito, *Biomaterials*, 2017, **30**, 709–718.
- 26 T. Ohara, K. Noma, S. Urano, S. Watanabe, S. Nishitani, Y. Tomono, F. Kimura, S. Kagawa, Y. Shirakawa and T. Fujiwara, *Int. J. Cancer*, 2013, **132**, 2705–2713.
- 27 R. Raveendran, J. P. Braude, E. Wexselblatt, V. Novohradsky, O. Stuchlikova, V. Brabec, V. Gandin and D. Gibson, *Chem. Sci.*, 2016, **7**, 2381–2391.
- 28 R. Zhang, X. Q. Song, R. P. Liu, Z. Y. Ma and J. Y. Xu, *J. Med. Chem.*, 2019, **62**, 4543–4554.
- 29 M. Feoktistova, P. Geserick and M. Leverkus, *Cold Spring Harb. Protoc.*, 2016, **2016**, 343–346.
- 30 E. N. Hoogenboezem and C. L. Duvall, *Adv. Drug Delivery Rev.*, 2018, **130**, 73–89.
- 31 A. Steinbrueck, A. C. Sedgwick, S.-M. Hwang, S. Sen, M. Y. Zhao, D.-Y. Huang, Y.-Y. Wang and J. L. Sessler, *Chemosensors*, 2021, **9**(4), DOI: 10.3390/chemosensors9040068.